

Plasmon-Enhanced Upconversion in Single $\text{NaYF}_4:\text{Yb}^{3+}/\text{Er}^{3+}$ Codoped Nanocrystals

Stefan Schietinger,^{*,†} Thomas Aichele,[†] Hai-Qiao Wang,[‡] Thomas Nann,[†] and Oliver Benson[‡]

[†]Nano-Optics, Institute of Physics, Humboldt-Universitaet zu Berlin, Hausvogteiplatz 5-7, D-10117 Berlin, Germany, and [‡]School of Chemistry, University of East Anglia (UEA), Norwich NR4 7TJ, U.K.

ABSTRACT In this Letter we report the plasmon-enhanced upconversion in single NaYF_4 nanocrystals codoped with $\text{Yb}^{3+}/\text{Er}^{3+}$. Single nanocrystals and gold nanospheres are investigated and assembled in a combined confocal and atomic force microscope setup. The nanocrystals show strong upconversion emission in the green and red under excitation with a continuous wave laser in the near-infrared at 973 nm. By the use of the atomic force microscope, we couple single nanocrystals with gold spheres (30 and 60 nm in diameter) to obtain enhanced upconversion emission. An overall enhancement factor of 3.8 is reached. A comparison of time-resolved measurements on the bare nanocrystal and the coupled nanocrystal–gold sphere systems unveil that faster excitation as well as faster emission occurs in the nanocrystals.

KEYWORDS Plasmon-enhanced, upconversion, nanocrystal, and Yb/Er codoped

Because of their great potential in a multitude of possible applications ranging from laser materials, near-infrared quantum counters, and biolabeling to lighting and display technologies,^{1–7} the development of new upconversion (UC) materials has recently drawn much attention. New routines in their synthesis opened the way to lanthanide-doped nanometer-sized crystals sharing the high efficiencies of their bulk equivalents.

The most promising materials are lanthanide-doped glassy or crystal materials sensitized by Yb^{3+} in which high-efficient multicolor UC in the green, red, and blue wavelength range can be observed from Er^{3+} and Tm^{3+} ions.^{8,9} The high UC yield in these substances is attributed to the very efficient mechanism of energy transfer UC,¹⁰ where the near-infrared photons are absorbed by the Yb^{3+} ions followed by subsequent energy transfers to Er^{3+} ions nearby (see Figure 1b). As no virtual states are involved, energy transfer UC can be more efficient by several orders of magnitude than other UC mechanisms like sum frequency generation, two-photon UC, or cooperative processes.¹¹ The crystal field and the phonon structure of the host matrix strongly influence the transitions of the lanthanides. Therefore, a change of the host can enhance or decrease significantly the UC luminescence and ongoing research is mainly concerned with the quest for host materials with increased conversion efficiencies.^{2,8,12–14}

Up to now, hexagonal (β -) phase NaYF_4 codoped with $\text{Yb}^{3+}/\text{Er}^{3+}$ is known to be the most effective upconverter,¹⁵ as the low maximal optical phonon energy in NaYF_4 suppresses nonradiative multiphonon relaxation processes, which can be responsible for a considerable reduction of the

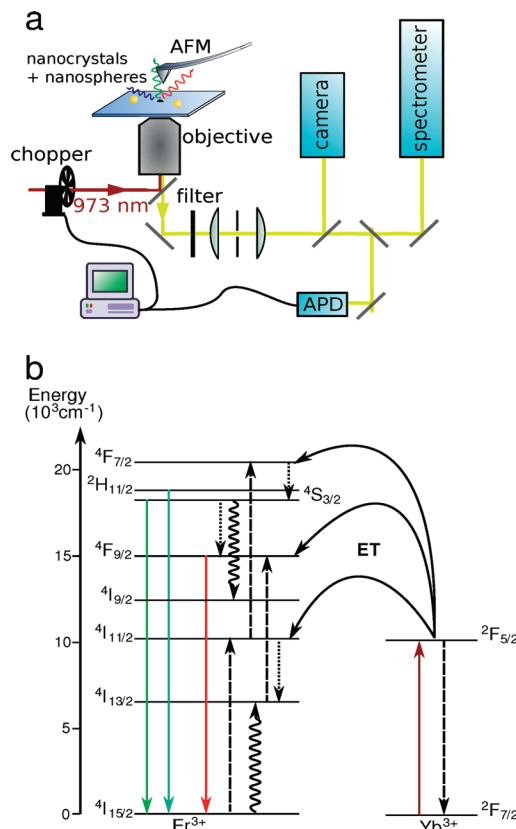


FIGURE 1. (a) Scheme of the experimental setup. On top of a homemade inverted microscope, an AFM allows manipulation. (b) Energy scheme with the relevant processes of energy transfer UC in $\text{Yb}^{3+}/\text{Er}^{3+}$ codoped materials: energy transfers, radiative, multiphonon processes, and cross-relaxation are depicted in dashed, full, dotted, and curly lines, respectively. The high efficiency in the UC is achieved by the subsequent absorption of the photons by the Yb^{3+} ions followed by the transfer of the excitation to the Er^{3+} .

* To whom correspondence should be addressed.

Received for review: 9/14/2009

Published on Web: 12/18/2009

emission intensity.⁸ These superior properties allow even their investigation on the single-nanocrystal (NC) level with moderate, continuous wave excitation.^{16,17} Furthermore, no bleaching or blinking is present, as the relevant fluorescence originates from well-shielded 4f electrons of the ions embedded in photostable crystals.

A well-known way to enhance fluorescence is the coupling of emitters to metallic surfaces or particles.^{18–23} In the vicinity of metal structures, the electric field distribution is altered, often referred to as local field effect. As a result, the excitation field as well as the emitted radiation can be enhanced, but also quenching by energy transfer and non-radiative relaxation in the metal is possible.^{18,19,24} Recently, the plasmon-enhancement of UC emission was reported by introducing silver nanoparticles in the glassy matrix hosting the lanthanide ions,^{25–27} but these experiments were done with random ensembles of the ions and the silver nanoparticles in the matrix. Another experiment used the UC of Er³⁺ ions to visualize enhanced nonlinear effects in a tapered plasmonic waveguide.²⁸ Also, a theoretical description of plasmon-enhancement of different UC processes was given very recently.²⁹

In contrast to these experiments, we demonstrate for the first time the controlled coupling of single NaYF₄ NCs to gold nanospheres of two different sizes. By monitoring the changes in the spectra as well as the changes in the rise and decay times of the UC fluorescence, we demonstrate that both excitation and emission are enhanced by the plasmonic structure.

The controlled nanoassembly is performed in a combined optical and atomic force microscope (AFM) setup which is sketched in Figure 1a. The homemade inverted confocal microscope allows optical characterization with diffraction limited resolution of the particles. In addition, the commercial AFM (Nanowizard I, JPK Instruments) on top allows size characterization below the diffraction limit in intermittent contact mode and assembly with up to nanometer precision in contact mode.

The codoped NCs are excited by a continuous wave Ti: sapphire laser (Coherent Mira 900, pumped by a Coherent Verdi V10) with 973 nm. The light is focused onto the NCs with the objective (Olympus Plan Apo, 60×, oil immersion) of the confocal microscope which also collects the UC emission. The excitation density is $\approx 2 \times 10^5 \text{ W cm}^{-2}$. The emitted light is filtered by Bragg filters (Linos Calflex) and can be detected either by an EMCCD camera (Andor iXon) or by an avalanche photodiode (APD) (PerkinElmer SPCM). The spectral composition of the UC fluorescence can be analyzed with a spectrograph (Princeton Instruments Acton 2500i with Andor iDus camera). For time-resolved measurements, a mechanical chopper (Standford Research SR540) is placed in the excitation path. The reference TTL signal from the chopper together with the APD detection pulses are recorded by a photon counting module (PicoQuant PicoHarp 300) in time-tagged time-resolved mode, and the obtained

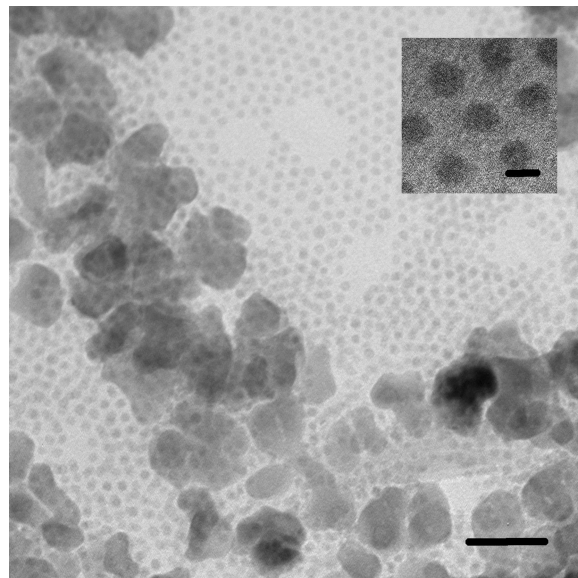


FIGURE 2. Transmission electron micrograph of a bimodal distribution of NaYF₄:Yb³⁺/Er³⁺ nanocrystals recorded on a JEOL 2000EX microscope at 200 kV. Scale bar: 50 nm (inset 5 nm).

data are processed by an open source program.³⁰ The chopper switches the laser on and off within 0.03 ms with a repetition rate of 400 Hz. To distinguish between the rise and decay times of green and red emission bands, additional filters are installed in the detection path.

A strictly bimodal set of UC nanoparticles was prepared by a microwave-assisted synthesis method. In a typical synthesis, 78 mg of sodium trifluoroacetate (TFA), 178 mg of yttrium-TFA, 43 mg of ytterbium-TFA, and 4.2 mg of erbium-TFA were dissolved in 6 mL of a 1:1 (v/v) mixture of oleic acid and octadecene. The mixture was heated to 120 °C under vigorous stirring. This solution was degassed and purged with nitrogen at least three times. Then it was transferred into the reacting vessel of a Discover LabMate microwave reactor (CEM, USA). The reaction mixture was irradiated with microwaves of a frequency of 2.45 GHz for 5 min with a maximum power of 300 W at 290 °C. The UC nanocrystals were collected by addition of an excess of absolute ethanol and centrifugation. Finally, they were dissolved in chloroform or toluene for transmission electron microscopy (TEM) characterization and further experiments. Figure 2 shows a TEM micrograph of a typical sample, containing UC nanocrystals of approximately 5 and 30 nm diameter. Only the larger nanocrystals were selected and investigated in the following experiments.

The samples are prepared by spin-coating the NCs on a coverslip followed by a second spin-coating step to deposit gold nanospheres. In the experiments presented here, two sizes of gold nanospheres with diameters of 30 and 60 nm (BBI GC 60 and GC 30) were used. With the help of the APD, a NC is placed in the confocal spot of the microscope. The AFM confirms that only a single NC with a height of 30 nm resides in the focal area. To find the particle in the laser focus

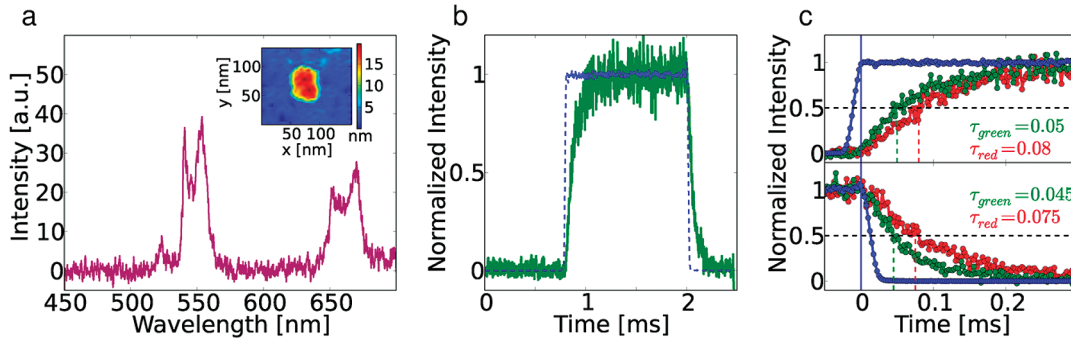


FIGURE 3. (a) UC spectrum of a single bare NC with the red and green emission bands. The inset shows the NC's image obtained with the AFM. (b) The green line shows the temporal evolution of the UC fluorescence (green part of emission) under chopped excitation. The blue dashed line represents the chopped intensity of the excitation laser. (c) The rise and the decay of the UC fluorescence in more detail: The blue dotted line is again the excitation laser intensity, the green and red dots represent the green and red emission.

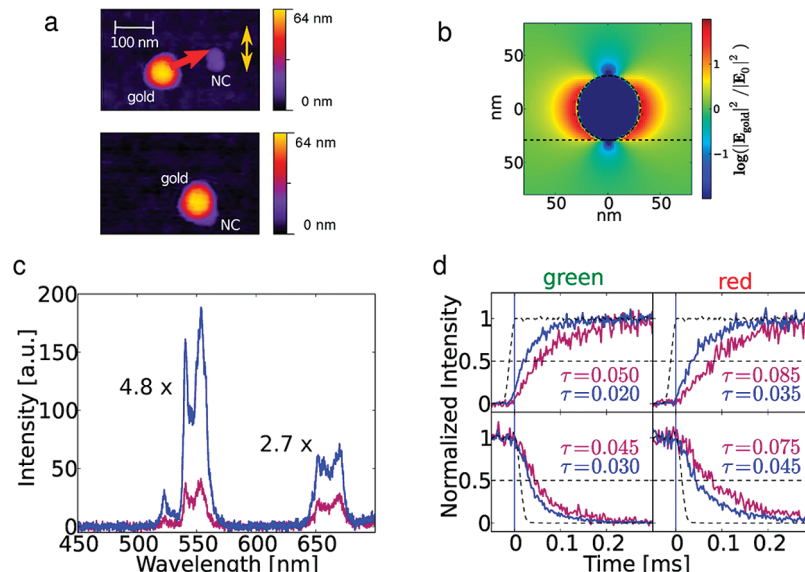


FIGURE 4. (a) AFM image showing the nanoassembly approach: The 60 nm gold nanosphere is attached to the NC with the help of the AFM tip. The yellow arrow indicates the polarization axis of the excitation light. (b) FDTD simulated intensity enhancement of the excitation light around a 60 nm gold sphere. (c) UC spectra of the NC without (violet curve) and with (blue curve) the gold nanosphere in close vicinity. The emission is strongly enhanced, the green part of the emission by a factor of 4.8, the red part by a factor of 2.7. The error is less than 2%. (d) Rise (upper) and decay (lower) of the green (left) and red (right) UC emission with the color code as in part c. Both the rise and the decay times are reduced due to coupling to the gold sphere. $t = 0$ is the time when the excitation laser reaches or leaves its maximum intensity.

area with the AFM, the AFM is first roughly adjusted by the shadow of its cantilever using the CCD camera, and then the sample is scanned. In order to ensure coincidence of the particle in the focus with a particle in the AFM scan, we move the particle in and out of the focus with the AFM, which causes a rise and fall of the optical signal detected by the APD.

In a first experiment, we explore the changes in the NC's emission introduced by a 60 nm gold sphere brought in its vicinity. Therefore at first, the UC fluorescence of the single bare NC is characterized; i.e., its spectrum and the emission rise and decay times of the green and red fluorescence, respectively, are measured. All NCs investigated were photostable for the experiment's duration. The red emission band (${}^4F_{9/2} \rightarrow {}^4I_{15/2}$) around 660 nm and the green emission bands (${}^2H_{11/2}, {}^4S_{3/2} \rightarrow {}^4I_{15/2}$) around 550 nm can be identified

in the spectrum of the NC, shown in Figure 3 a. The temporal evolution of the UC signal is shown in Figure 3b for the green part of the emission. As neither the rise nor the decay time of the fluorescence is monoexponential, we determine the time τ for the signal to rise (decay) to half of its maximal value. The rise and decay times of the green and red emission bands are depicted in Figure 3c, respectively. The green UC fluorescence in the codoped NCs shows shorter rise and decay times than the red UC fluorescence.

After characterization of the bare NC, a 60 nm gold sphere is brought in the vicinity of the NC with the AFM in contact mode (see Figure 4a). It is important to align the gold sphere in an appropriate position, as the field enhancement around the sphere critically depends on the polarization of the excitation light. Therefore, the axis defined by the centers of the gold sphere and NC have to be aligned along

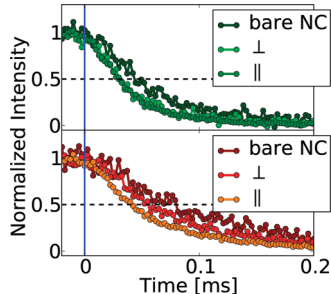


FIGURE 5. Excitation-polarization dependence of the green (upper) and the red (lower) decay times. The lifetime of the green UC fluorescence does not show any difference for the excitation polarization tuned to maximal (\parallel) or minimal (\perp) intensity, while the lifetime of the red UC fluorescence is smaller in the case of tuning to maximal intensity. For comparison, also the decay time of the bare NC is shown.

the polarization axis. After the position of the gold sphere is optimized, the spectral properties and dynamics of the emission of the coupled gold-NC system are recorded. The spectrum of the coupled system is shown in Figure 4c (blue curve). For comparison the emission spectrum of the bare NC is shown (violet curve) as well. The emission is drastically enhanced; the overall emission is increased by a factor of 3.8. However, the enhancement is not equal for both emission bands: While the red emission increases by a factor of 2.7, the green emission is 4.8 times stronger than before. The error of the enhancement factors is less than 2%. The plasmonic enhancement effect on the emission of the NC is also reflected in a reduction of the rise and decay times (see Figure 4c).

The enhancement factors vary strongly with the exact position of the gold nanosphere with respect to the NC and the polarization axis of the excitation light. For different configurations and different NCs, values between 2 and 4.8 and 1.6 and 2.7 were observed for green and red UC fluorescence, respectively. The highest values observed here are not a fundamental limit; improvement is still possible, e.g., by changing the size or shape of the NCs and the gold particles.

The amplification of the emission observed is much higher than the one predicted by Esteban et al.,²⁹ which is around unity for energy transfer upconversion. We ascribe this to the fact that the full complexity of the level system is not covered in their model. Furthermore, we cannot exclude excited-state absorption under the high excitation densities present in the confocal configuration. The comparison of codoped NCs and NCs solely doped with Er³⁺ under equal excitation conditions in a confocal setup will be the subject of future studies.

There are two effects that contribute to the rise time reduction: First, the excitation intensity at the location of the NC is enhanced. The change of the excitation field intensity is illustrated in Figure 4b by a 3D FDTD simulation using the Lumerical FDTD Solutions package. Second, the coupling to the plasmon resonance of the 60 nm gold sphere at around

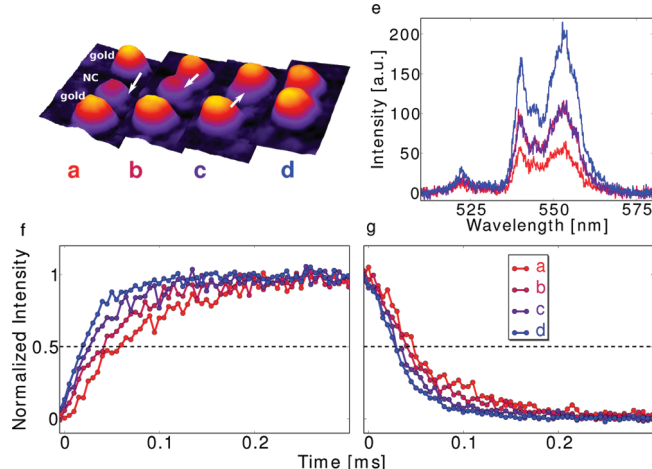


FIGURE 6. (a–d) A NC of 25 nm in diameter is stepwise sandwiched between two gold spheres of 30 nm in diameter. The arrows indicate how the gold nanospheres moved toward the NC. (e, f, and g): Rise and lifetime of the green emission for the different configurations. The emission is enhanced from configuration a to b, but further decreasing the NC-gold sphere distance does not enhance the emission anymore as quenching eats up the amplification effects. This is reflected in the rise and lifetimes. The second gold sphere doubles the emission and further reduces rise and lifetime.

540 nm can also amplify the transitions which involve the second energy transfer step to reach the $^4F_{7/2}$ and the $^4F_{9/2}$, respectively.

The coupling to the plasmon also explains the reduced decay time of the green and red emitting levels: On the one hand, the radiative rate can be enhanced, but the gold sphere introduces an additional nonradiative decay channel. These effects result in shorter lifetimes of the levels and thus a more rapid decay of the fluorescence signal.

As the plasmon resonance around 540 nm of the gold sphere overlaps stronger with the green emission band, one would indeed expect a stronger influence on the green emission process. However, the different enhancement factors for the green and red emission band can be more likely explained by the change in the excitation scheme: If the excitation power is increased, it becomes more probable that a second energy transfer step further excites the Er³⁺ ion by the transition $^4I_{11/2} \rightarrow ^4F_{7/2}$ before the nonradiative decay $^4I_{11/2} \rightarrow ^4I_{13/2}$ can take place, which is an intermediate step to fill the red-emitting $^4F_{9/2}$ level.

To explore whether the decay time changes are induced by the varied excitation conditions, we rotate the excitation polarization with a $\lambda/2$ -plate and detect the emission on its maximum and minimum values (see Figure 5). The green emission shows no change in the decay time between different excitation polarizations. However, the decay time of the red emission is longer in the case of the polarization tuned to minimal emission intensity, but both lifetimes are shorter than that for the bare NC. This behavior strongly indicates that the population path for the red emitting level is altered with the excitation intensity.

In a second experiment, a single NC with a height of 25 nm is subsequently sandwiched between two 30 nm gold spheres in three steps (see Figure 6a–d). The emission is studied in each configuration, parts a–d. In configuration a, the gold nanospheres and the NC are well separated by a gap of more than 20 nm so that the NC's emission is only marginally influenced by the spheres (Figure 6a). Then one of the gold spheres is moved toward the NC (Figure 6b). As expected, the emission is enhanced and the rise and decay times are reduced. This is shown for the green emission in Figure 6e,f. By bringing a gold nanosphere in full contact with the NC (Figure 6c), the rise and decay times are further decreased, while the overall emission intensity is unchanged. This can be explained by the following consideration: In configuration b, excitation and emission are enhanced, and the gold sphere is still too far to introduce quenching of the emission. However, in full contact, additional quenching eats up any further amplification of the fluorescence. The second particle (see Figure 6) doubles the effect of the first particle: The intensity of the sandwich configuration d is 1.8 times as high as those in the configurations b and c and 3.2 times as high as that in configuration a. The error is again below 2 %.

In conclusion, we have performed upconversion spectroscopy on single $\text{NaYF}_4:\text{Yb}^{3+}/\text{Er}^{3+}$ codoped NCs. By controlled nanoassembly of these NCs with gold nanospheres, we could demonstrate the enhancement of upconversion fluorescence by the employment of plasmonic effects. Rise and decay time measurements revealed that both the excitation and the emission processes are influenced by the coupling to plasmon resonance in the gold sphere. FDTD simulations confirmed that even though the excitation light is rather far from the plasmon resonance, the excitation intensity is considerably enhanced. Therefore, even single plasmonic nanostructures can help to further increase the efficiency of UC processes without spoiling the fluorescence yield by quenching. The controlled studies of UC performed here will provide important input for the optimum design of future hybrid UC particles consisting of $\text{NaYF}_4:\text{Yb}^{3+}/\text{Er}^{3+}$ nanocrystals and metal nanostructures. These particles will have enhanced UC efficiency and may even be fabricated on a larger scale using only chemical synthesis.

Acknowledgment. Financial support was given by the DFG, SFB 448, and project IQOSuPla.

REFERENCES AND NOTES

- (1) Schepes, R. *Prog. Quantum Electron.* **1996**, *20*, 271–358.
- (2) Yi, G.; Lu, H.; Zhao, S.; Ge, Y.; Yang, W.; Chen, D.; Guo, L. *Nano Lett.* **2004**, *4*, 2191–2196.
- (3) Lim, S.; Riehn, R.; Ryu, W.; Khanarian, N.; Tung, C.; Tank, D.; Austin, R. *Nano Lett.* **2006**, *6*, 169–174.
- (4) Phillips, M.; Hehlen, M.; Nguyen, K.; Sheldon, J.; Cockroft, N. Upconversion phosphors: Recent advances and new applications. *Physics and Chemistry of Luminescent Materials: Proceedings of the Eighth International Symposium*, 2000.
- (5) Downing, E.; Hesselink, L.; Ralston, J.; Macfarlane, R. *Science* **1996**, *273*, 1185–1189.
- (6) Joubert, M. *Opt. Mater.* **1999**, *11*, 181–203.
- (7) Shalav, A.; Richards, B.; Trupke, T.; Krämer, K.; Güdel, H. *Appl. Phys. Lett.* **2005**, *86*, No. 013505.
- (8) Heer, S.; Kömppe, K.; Güdel, H.-U.; Haase, M. *Adv. Mater.* **2004**, *16*, 2102–2105.
- (9) Ehrlert, O.; Thomann, R.; Darbandi, M.; Nann, T. *ACS Nano* **2008**, *2*, 120–124.
- (10) Auzel, F. *C. R. Hebd. Séances Acad. Sci.* **1966**, *263b*, 819.
- (11) Auzel, F. *Chem. Rev.* **2004**, *104*, 139–173.
- (12) Krämer, K.; Biner, D.; Frei, G.; Güdel, H.; Hehlen, M.; Lüthi, S. *Chem. Mater.* **2004**, *16*, 1244–1251.
- (13) Zeng, J.; Su, J.; Li, Z.; Yan, R.; Li, Y. *Adv. Mater.* **2005**, *17*, 2119–2123.
- (14) Chen, G.; Liu, H.; Liang, H.; Somesfalean, G.; Zhang, Z. *J. Phys. Chem. C* **2008**, *112*, 12030–12036.
- (15) Schäfer, H.; Ptacek, P.; Kömppe, K.; Haase, M. *Chem. Mater.* **2007**, *19*, 1396–1400.
- (16) Schietinger, S.; Menezes, L.; Lauritzen, B.; Benson, O. *Nano Lett.* **2009**, *9*, 2477–2481.
- (17) Wu, S.; Han, G.; Milliron, D.; Aloni, S.; Altoe, V.; Talapin, D.; Cohen, B.; Schuck, P. *Proc. Natl. Acad. Sci. U.S.A.* **2009**, *106*, 10917.
- (18) Glass, A.; Liao, P.; Bergman, J.; Olson, D. *Opt. Lett.* **1980**, *5*, 368.
- (19) Lakowicz, J. *Anal. Biochem.* **2001**, *298*, 1–24.
- (20) Shimizu, K.; Woo, W.; Fisher, B.; Eisler, H.; Bawendi, M. *Phys. Rev. Lett.* **2002**, *89*, 117401.
- (21) Pompa, P.; Martiradonna, L.; Della Torre, A.; Della Sala, F.; Manna, L.; De Vittorio, M.; Calabi, F.; Cingolani, R.; Rinaldi, R. *Nat. Nanotechnol.* **2006**, *1*, 126–130.
- (22) Bek, A.; Jansen, R.; Ringler, M.; Mayilo, S.; Klar, T.; Feldmann, J. *Nano Lett.* **2008**, *8*, 485–490.
- (23) Schietinger, S.; Barth, M.; Aichele, T.; Benson, O. *Nano Lett.* **2009**, *9*, 1694–1698.
- (24) Dulkeith, E.; Morteani, A.; Niedereichholz, T.; Klar, T.; Feldmann, J.; Levi, S.; van Veggel, F.; Reinhoudt, D.; Möller, M.; Gittins, D. *Phys. Rev. Lett.* **2002**, *89*, 20.
- (25) Kassab, L.; de Araújo, C.; Kobayashi, R.; de Almeida Pinto, R.; da Silva, D. *J. Appl. Phys.* **2007**, *102*, 103515.
- (26) Kassab, L.; Bomfim, F.; Martinelli, J.; Wetter, N.; Neto, J.; de Araújo, C. *Appl. Phys. B: Lasers Opt.* **2009**, *94*, 239–242.
- (27) Rai, V.; Menezes, L.; de Araújo, C.; Kassab, L.; da Silva, D.; Kobayashi, R. *J. Appl. Phys.* **2008**, *103*, No. 093526.
- (28) Verhagen, E.; Kuipers, L.; Polman, A. *Nano Lett.* **2007**, *7*, 334–337.
- (29) Esteban, R.; Laroche, M.; Greffet, J. *J. Appl. Phys.* **2009**, *105*, No. 033107–033107.
- (30) Jones, E.; Oliphant, T.; Peterson, P.; et al. SciPy: Open source scientific tools for Python, 2001 <http://www.scipy.org/>.